Available online at www.sciencedirect.com
SCIENCE DIRECT®
Earth and Planetary Science Letters 237 (2005) 768–780
EPSL
www.elsevier.com/locate/epsl

Transformation of lithospheric mantle through peridotite-melt reaction: A case of Sino-Korean craton

Hong-Fu Zhang

State Key Laboratory of Lithospheric Evolution, Institute of Geology and Geophysics, Chinese Academy of Sciences, P.O. Box 9825, Beijing 100029, PR China

Received 8 June 2004; received in revised form 15 April 2005; accepted 24 June 2005
Available online 2 August 2005
Editor: E. Boyle

Abstract

Early Cretaceous Fangcheng basalts, erupted in Luxi region of Shandong Province, China, contain olivine xenocrysts with clear compositional zonations, which provide evidence for important mantle-melt reactions. These zoned olivines are fine-grained (200~900 μm) and the core of the relatively larger grains have compositions (such as Mg#=88~92) similar to those of olivines from the mantle peridotitic xenoliths entrained in Cenozoic basalts from the Sino-Korean craton and their rims (Mg#=76~83) are compositionally close to those of the olivine phenocrysts from the host basalts. These compositional features as well as textural characteristics such as rounded and embayed crystal shape, well-developed cracks and grain sizes demonstrate that these olivines are mantle xenocrysts disaggregated from the lithospheric peridotites. The zoned texture was formed through rapid reaction between olivine and host melt. This may suggest that mantle-melt reaction was once very significant in the Mesozoic lithospheric mantle beneath the southeastern portion of the Sino-Korean craton, which we consider to be responsible for the replacement of lithospheric mantle from the Paleozoic refractory (high-Mg) peridotitic mantle to the late Mesozoic fertile (low-Mg) and enriched mantle with the loss of more than 120 km Archaean lithospheric keel in the region.

Keywords: olivine xenocryst; peridotite-melt reaction; lithospheric mantle; Sino-Korean craton

1. Introduction

Olivine, $(Mg, Fe, Ni, Mn)_2SiO_4$, the predominant mineral phase in the Earth's upper mantle [1,2], is present in a wide range of mafic volcanic rocks such as kimberlites, lamproites, and basalts as phenocryst and/or xenocryst [3–7]. Changes of physic properties of olivine in the mantle, for instance, deformation-induced lattice preferred orientation and phase transformation [8–11], were believed to be responsible for deep-focus earthquakes. Compositional changes of olivine in the lithospheric mantle could also be important in the initiation of the earthquakes in the intra-continental plate and in the evolution of the lithospheric mantle, for instance, in the Archaean

E-mail address: hfzhang@mail.igcas.ac.cn.

0012-821X/$ - see front matter © 2005 Elsevier B.V. All rights reserved.
doi:10.1016/j.epsl.2005.06.041

Sino-Korean craton. Olivine chemical zonation found in the Mesozoic Fangcheng basalts from the Archaean Sino-Korean craton provides evidence for the replacement of lithospheric mantle through peridotite-melt reaction. This replacement could result in the transformation of the lithospheric mantle from high-Mg peridotites to low-Mg peridotites plus pyroxenite veins and finally the loss of more than 120 km Archaean lithospheric keel in the region.

2. The Sino-Korean craton

Considerable studies have showed that the Archaean Sino-Korean craton has a unique history, where the lithosphere lost its thickness of more than 120 km within 200 Ma [12–21]. This lithospheric loss was also accompanied with the compositional change from the old refractory to young fertile lithosphere. Investigation of Mesozoic basalts and mafic intrusions in the southeastern portion of the Sino-Korean craton indicates that the Mesozoic time was the major period of the lithospheric loss in the region. These intracontinental volcanic rocks and mafic intrusions have very similar geochemical features, such as high Si, Mg, Ca and low alkalis, Ti and Al, strong enrichment in LREE and LILE (Rb, Ba, U, Th), depletion in HFSE (Nb, Ta, Zr, Hf), high initial $^{87}Sr/^{86}Sr$ and low $^{143}Nd/^{144}Nd$ and $^{206}Pb/^{204}Pb$ isotopic ratios. These geochemical features require that the sources for these Mesozoic

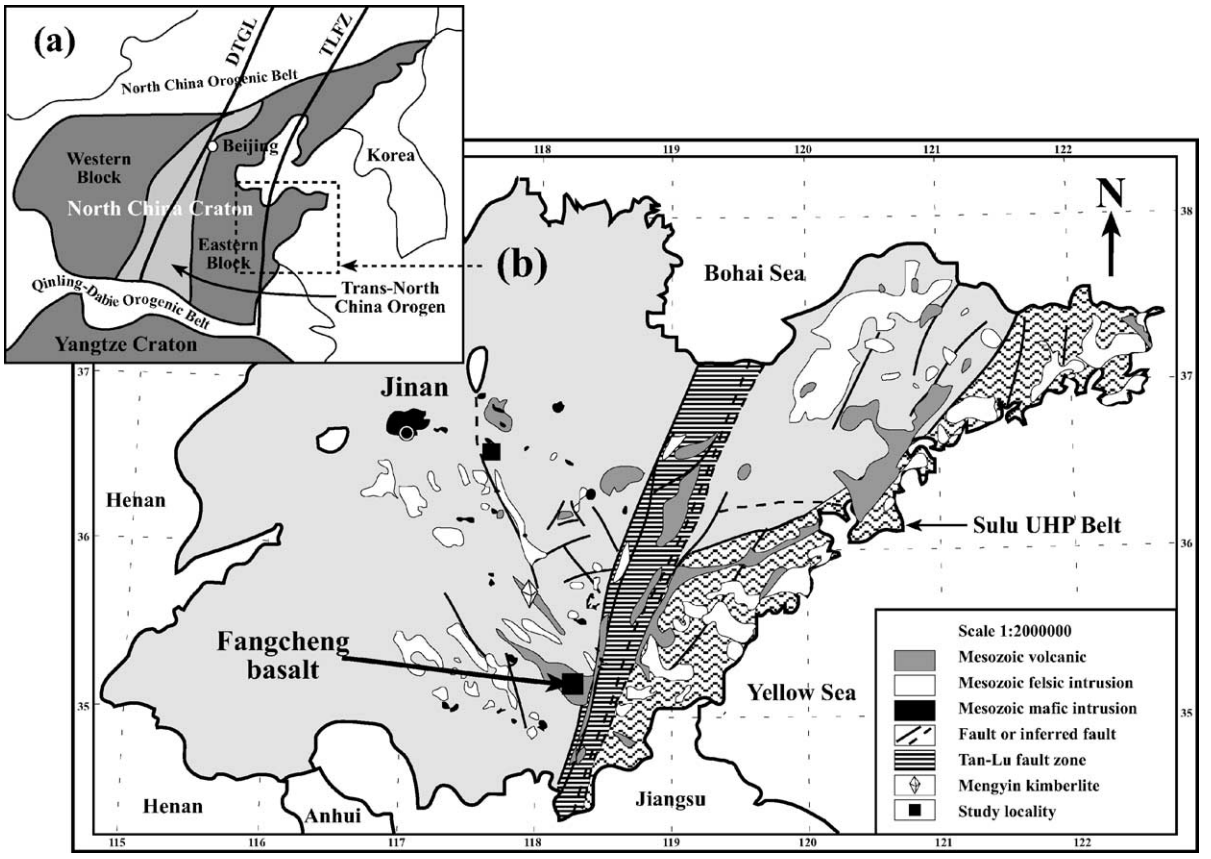

Fig. 1. (a) Simplified geological map shows the major tectonic devision of the North China craton (Zhao et al. 2001), a part of Sino-Korean craton. The Daxing'anling-Taihangshan Gravity Anomaly Line (DTGL) is parallel to the Trans-North China Orogen. The study area, Shandong Province, is situated in the eastern block of the North China craton. (b) Distribution of Mesozoic intrusive and volcanic rocks in Shandong Province, as well as Paleozoic Mengyin diamondiferous kimberlite. The Tan-Lu Fault Zone (TLFZ) separates the Eastern Block into two parts: Luxi and Jiaodong devisions.

mafic rocks were the lithospheric mantle which had been highly affected by the crustal materials [20–23]. Subduction of the Yangtze Craton was invoked, and the compositional change of the lithospheric mantle was suggested to be completed by the peridotite-melt reaction induced by the circum-craton subduction [20–22]. Here we provide more direct evidence that comes from the mantle xenocryst entrained in the Mesozoic Fangcheng basalts.

3. Background geology

The Archean Sino-Korean craton is divided by a Proterozoic orogenic belt, the Trans-North China Orogen, into two parts, the Eastern and Western Blocks [24]. This craton is bounded in the south by the Qinling-Dabie-Sulu orogenic belt [25,26] and in the north by the Central Asian orogenic belt [27] (Fig. 1a). The Qinling-Dabie-Sulu orogenic belt resulted from continental collision between the Yangtze craton and the Sino-Korean craton in the Triassic [25]. The occurrence of diamond and coesite in the eclogites [28], the finding of coesite inclusions in zircons from ortho- and para-gneisses [29], and the exsolution lamellae of clinopyroxene, rutile and apatite in garnets from the eclogite all demonstrate that the upper and middle crustal units of the Yangtze craton were once subducted to ultrahigh pressure conditions at depths greater than 200 km [30]. The deep subduction of the Yangtze craton and its subsequent collision with the Sino-Korean craton significantly affected the lithospheric mantle beneath the southeastern portion of the Sino-Korean craton. The melts from the subducted crustal materials fertilized the overlying lithospheric mantle underneath the Sino-Korean craton, as documented in the Mesozoic lithosphere-derived basaltic rocks of the region [20,22,23].

A long-lived wrench fault zone [31], the Tan-Lu fault, separates the Shandong Province into two

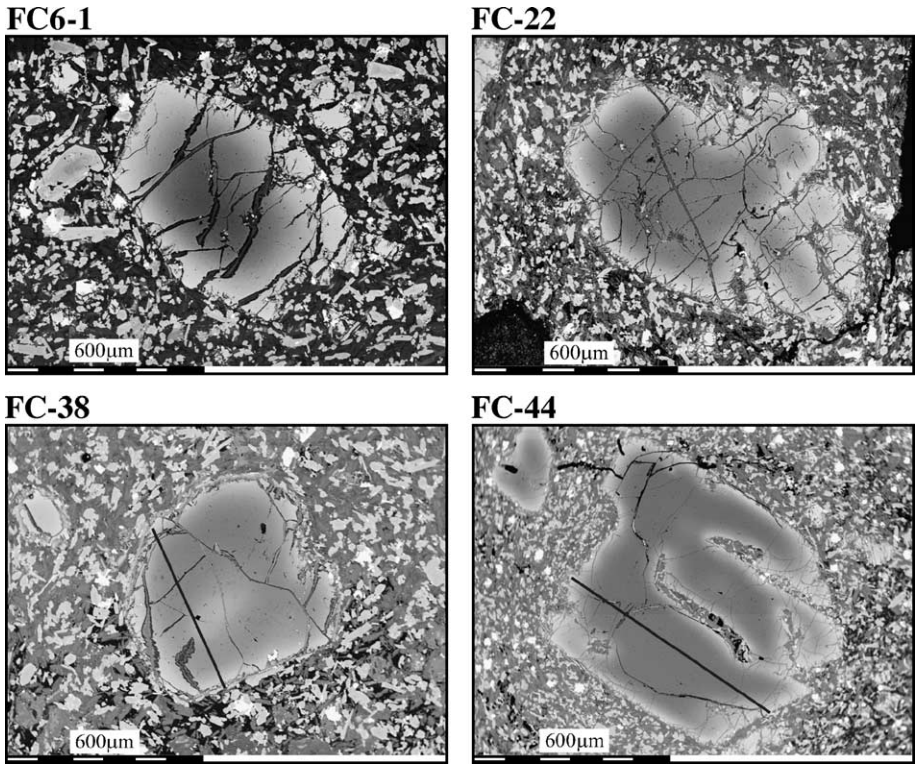

Fig. 2. Backscattered image for zoned olivine. Dark line shows the EPMA traverse in Fig. 3 (FC-38, FC-44).

parts (Fig. 1b), the western part is traditionally called as Luxi region and the eastern as Jiaodong. Mesozoic basaltic-trachyandesitic volcanics and dioritic-granitoid intrusions are well distributed in both the Luxi and Jiaodong regions (Fig. 1b), however mafic intrusions are dominantly scattered in the Luxi region. The Cretaceous Fangcheng basalts which contain olivine xenocrysts are situated in Luxi region (Fig. 1b).

4. Mesozoic basalts

Mesozoic Fangcheng basalts, about 70 km west of the giant Tan-Lu wrench fault, are distributed within a small Mesozoic sedimentary fault-bounded basin, Feixian county of Shandong Province. These basalts stratigraphically belong to the Qingshan Formation and erupted at 125 Ma [20]. The basalts have porphyritic texture and massive structure, and can be classified as alkaline basalt and olivine tholeiite based on the major element compositions. Porphyritic mineral grains are sparse and composed dominantly of olivines (about 5%) including xenocrysts and phenocrysts and few clinopyroxene xenocrysts (less than 2%). Detailed petrology and geochemistry for these basalts have been previously reported [20]. Fangcheng basalts contain a large number of spinel-facies ultramafic xenoliths. The xenoliths are in the range of 1~8 cm and dominantly composed of clinopyroxene with minor olivine, orthopyroxene, spinel and plagioclase, thus they are named as olivine clinopyroxenites. These pyroxenites show clearly accumulative structure.

5. Olivine mineralogy

Olivine xenocrysts occur in olivine tholeiites (Fig. 2). They are sparse (about 3%) and small (<1 mm, normally in the range of 200~900 μm). Majorities of olivine xenocrysts have erosion textures such as rounded shapes and eroded embayment (Fig. 2). All olivine xenocrysts have clear compositional zonation. In backscattered images, it shows darker color in the core (Mg-rich) and lighter in the rim (Fe-rich). The widths of the core and the rim vary among grains. Generally, the larger grains have thinner rims and the smaller grains have wider rims (Figs. 2 and 3). In contrast, olivine phenocrysts in the tholeiites are more abundant without apparent zonation and dominantly occur as subhedral and coarse grains (majorities in the range of 1–2 mm). Olivines in the matrix of the tholeiite are anhedral and tiny (less than 200 μm). Olivines in the pyroxenite xenolith occur as

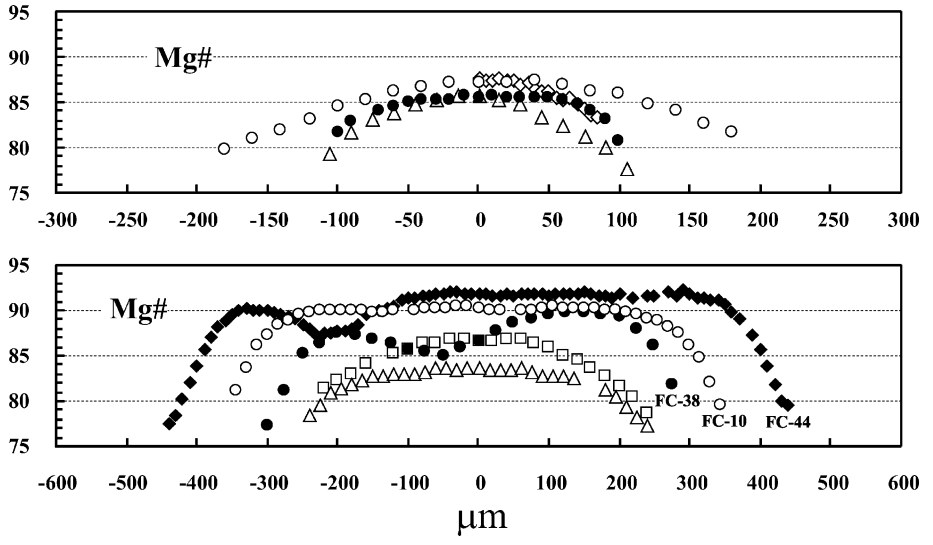

Fig. 3. Mg# traverse for zoned olivine. Mg#=Mg/(Mg+Fe)*100.

Table 1
Representative analyses of zoned olivine xenocrysts from Mesozoic Fangcheng basalts

Olivine	Xenocryst	SiO_2	Cr_2O_3	MgO	CaO	MnO	FeO	NiO	Mg#
FC6-1	core	40.21	0.12	48.07	0.11	0.12	10.77	0.60	88.8
	mantle	40.17	0.10	46.68	0.16	0.16	12.24	0.49	87.2
	rim	38.83	0.05	39.21	0.27	0.32	21.08	0.24	76.8
FC8-1	core	41.06	0.10	47.93	0.10	0.12	10.37	0.32	89.2
	mantle	39.56	0.07	42.07	0.11	0.35	17.56	0.28	81.0
	rim	39.64	0.03	40.77	0.16	0.37	18.86	0.18	79.4
FC18-1	core	40.88	0.11	49.27	0.11	0.10	9.04	0.50	90.7
	rim	39.66	0.30	44.07	0.17	0.22	15.35	0.23	83.7
FC-2	core	39.97	0.10	48.93	0.16	0.12	10.53	0.20	89.2
	mantle	39.44	0.01	46.62	0.17	0.24	13.24	0.29	86.3
	rim	38.06	0.01	41.40	0.18	0.31	19.90	0.14	78.8
FC-14	core	40.33	0.06	49.00	0.15	0.13	10.04	0.29	89.7
	mantle	39.75	0.01	46.77	0.12	0.18	12.88	0.29	86.6
	rim	38.70	0.00	42.53	0.16	0.31	18.10	0.20	80.7
FC-26	core	39.06	0.01	46.09	0.15	0.16	14.30	0.23	85.2
	mantle	38.89	0.04	44.17	0.15	0.25	16.13	0.36	83.0
	rim	38.47	0.02	43.42	0.16	0.28	17.48	0.18	81.6
FC-29	core	39.19	0.22	47.09	0.20	0.17	12.81	0.34	86.8
	mantle	39.22	0.02	45.81	0.14	0.19	14.25	0.37	85.1
	rim	38.62	0.06	42.93	0.19	0.22	17.73	0.27	81.2
FC-31	core	39.49	0.02	47.38	0.12	0.14	12.54	0.31	87.1
	rim	38.14	0.03	41.15	0.19	0.32	20.04	0.14	78.5
FC-35	core	38.58	0.03	50.77	0.14	0.12	9.99	0.37	90.1
	mantle	38.28	0.00	42.39	0.15	0.27	18.68	0.23	80.2
	rim	38.36	0.00	40.93	0.20	0.30	20.09	0.12	78.4
FC-36	core	39.84	0.08	47.91	0.13	0.15	11.55	0.34	88.1
	core 2	39.07	0.04	46.01	0.13	0.22	14.21	0.32	85.2
	mantle	38.46	0.03	43.50	0.16	0.28	17.32	0.26	81.7
	rim 2	38.15	0.09	41.75	0.19	0.31	19.25	0.25	79.5
	rim	38.24	0.01	40.14	0.27	0.34	20.92	0.09	77.4
FC-39	core	40.20	0.09	49.38	0.14	0.10	9.75	0.33	90.0
	mantle	38.84	0.04	44.59	0.15	0.20	15.93	0.25	83.3
	rim	38.18	0.05	39.60	0.25	0.29	21.44	0.19	76.7
FC-41	core	39.51	0.08	48.19	0.15	0.13	11.70	0.23	88.0
	mantle	39.65	0.02	46.79	0.14	0.16	12.96	0.28	86.6
	rim	38.19	0.04	42.05	0.18	0.27	19.04	0.23	79.7
FC-44	core	40.32	0.05	50.87	0.12	0.11	8.06	0.48	91.8
	mantle	40.46	0.06	50.65	0.11	0.11	8.13	0.49	91.7
	rim	38.32	0.06	40.24	0.23	0.30	20.71	0.14	77.6

Olivine	μm	SiO_2	Cr_2O_3	MgO	CaO	MnO	FeO	NiO	Mg#
Line analyses									
FC-4	−180	38.59	2.23	40.04	0.41	0.47	18.24	0.02	79.7
	−160	38.64	0.06	43.29	0.20	0.36	17.30	0.16	81.7
	−120	38.73	0.18	44.00	0.19	0.28	16.51	0.11	82.6
	−80	41.00	0.33	44.39	0.21	0.19	13.67	0.21	85.3
	−40	39.64	0.35	46.53	0.18	0.28	12.83	0.20	86.6
	0	39.46	0.00	47.38	0.15	0.18	12.53	0.31	87.1
FC-10	0	40.08	0.01	49.59	0.16	0.19	9.64	0.34	90.2
	60	39.95	0.03	49.42	0.17	0.21	9.89	0.33	89.9
	120	40.04	0.03	49.70	0.16	0.21	9.56	0.30	90.3
	180	39.37	0.19	49.34	0.21	0.18	10.38	0.34	89.9

Table 1 (*continued*)

Olivine	μm	SiO_2	Cr_2O_3	MgO	CaO	MnO	FeO	NiO	Mg#
Line analyses									
FC-10	240	39.92	0.05	48.75	0.14	0.17	10.67	0.30	89.1
	270	39.93	0.05	47.96	0.13	0.22	11.43	0.28	88.2
	300	39.55	0.03	46.48	0.15	0.27	13.26	0.27	86.2
	315	39.17	0.02	45.56	0.16	0.30	14.53	0.27	84.8
	330	38.66	0.03	43.68	0.19	0.36	16.87	0.20	82.2
	345	38.14	0.03	41.80	0.22	0.42	19.24	0.14	79.5
FC-14	−105	38.25	0.07	41.48	0.25	0.46	19.31	0.17	79.3
	−90	38.22	0.05	43.48	0.21	0.38	17.43	0.24	81.6
	−75	38.46	0.08	44.49	0.15	0.34	16.25	0.24	83.0
	−60	38.40	0.06	45.18	0.15	0.36	15.59	0.26	83.8
	−45	38.86	0.07	45.61	0.18	0.29	14.71	0.28	84.7
	−30	38.82	0.70	45.55	0.19	0.27	14.17	0.30	85.1
	−15	39.05	0.08	46.38	0.14	0.29	13.71	0.34	85.8
	0	38.91	0.11	46.44	0.13	0.31	13.82	0.28	85.7
FC-22	0	39.35	0.12	47.07	0.13	0.21	12.86	0.26	86.7
	40	39.29	0.03	47.46	0.13	0.19	12.70	0.19	86.9
	80	39.17	0.08	46.94	0.13	0.12	13.32	0.25	86.3
	120	37.62	1.31	45.80	0.36	0.29	14.44	0.19	85.0
	160	38.84	0.04	44.88	0.11	0.40	15.55	0.18	83.7
	200	38.63	0.00	43.23	0.18	0.34	17.43	0.18	81.5
	240	37.59	0.11	41.45	0.24	0.42	20.09	0.11	78.6
FC-24	0	39.52	0.05	48.05	0.15	0.21	12.00	0.02	87.7
	20	39.42	0.06	47.95	0.18	0.13	12.25	0.00	87.5
	40	39.31	0.06	47.19	0.15	0.18	13.10	0.02	86.5
	60	39.16	0.13	46.13	0.14	0.23	14.13	0.08	85.3
	70	39.02	0.00	45.75	0.15	0.31	14.68	0.09	84.8
	80	38.86	0.14	44.93	0.16	0.18	15.69	0.04	83.6
	85	38.47	0.06	44.92	0.15	0.24	16.11	0.05	83.3
FC-38	−300	39.14	0.09	39.07	0.40	0.46	20.64	0.19	77.1
	−275	39.25	0.07	42.46	0.29	0.37	17.37	0.20	81.2
	−250	39.35	0.05	45.79	0.18	0.29	14.14	0.21	85.2
	−225	39.28	0.10	46.82	0.17	0.25	13.13	0.25	86.4
	−200	39.21	0.15	47.85	0.17	0.20	12.12	0.30	87.6
	−175	39.13	0.11	47.67	0.17	0.18	12.45	0.29	87.2
	−150	39.05	0.08	47.49	0.17	0.16	12.78	0.27	86.9
	−125	39.04	0.07	47.00	0.17	0.23	13.26	0.23	86.3
	−100	39.03	0.07	46.50	0.17	0.30	13.74	0.19	85.8
	−75	39.10	0.05	46.16	0.16	0.26	14.08	0.19	85.4
	−50	39.18	0.04	45.82	0.14	0.22	14.41	0.19	85.0
	−25	39.30	0.05	46.41	0.15	0.22	13.66	0.22	85.8
	0	39.42	0.06	47.01	0.15	0.23	12.89	0.24	86.7
FC-44	0	40.46	0.06	50.65	0.11	0.10	8.13	0.49	91.7
	50	40.50	0.07	50.43	0.13	0.09	8.29	0.49	91.6
	100	40.30	0.04	50.57	0.12	0.10	8.34	0.52	91.5
	150	40.62	0.06	50.77	0.10	0.08	7.94	0.43	91.9
	200	40.61	0.07	50.61	0.12	0.09	8.01	0.50	91.8
	250	40.37	0.10	50.67	0.11	0.11	8.23	0.41	91.7
	300	40.49	0.08	50.62	0.12	0.09	8.14	0.46	91.7
	350	40.41	0.07	49.72	0.11	0.13	9.15	0.41	90.6
	370	39.98	0.08	49.18	0.12	0.22	9.98	0.44	89.8
	390	39.36	0.01	47.56	0.14	0.18	12.45	0.31	87.2

(continued on next page)

Table 1 (*continued*)

Olivine	μm	SiO_2	Cr_2O_3	MgO	CaO	MnO	FeO	NiO	Mg#
Line analyses									
FC-44	410	39.02	0.00	44.80	0.14	0.28	15.49	0.28	83.8
	430	38.11	0.01	42.32	0.21	0.38	18.75	0.22	80.1
	440	38.51	0.06	41.73	0.21	0.40	19.00	0.08	79.5

Composition was recalculated to 100%.

interstitial grains among large pyroxene grains and are small (100~200 μm) without zonation. Cracks and fractures are common in the olivine xenocrysts, distinctive from their counterparts such as phenocrysts, matrix minerals, and interstitial grains in the xenoliths.

6. Olivine chemistry

Major element compositions of olivines and backscattered images were obtained with a Cameca SX50 at the Institute of Geology and Geophysics, Chinese Academy of Sciences and with a JEOL JXA-8900R Superprobe) at Geological Survey of Japan, respectively. Analyses were performed with a beam of 15 KeV and 20 nA focused on a spot ~2 mm in diameter. The representative analyses are given in Table 1.

Olivine xenocrysts show apparently compositional zonation (Figs. 3 and 4). The cores are generally higher in MgO and NiO contents and lower in FeO, MnO and CaO contents relative to the rims (Table 1), with their Mg# (88~92) in larger grains similar to those of olivines from peridotitic xenoliths entrained in Cenozoic basalts of the craton (Fig. 5). MgO and NiO contents decrease and FeO, MnO and CaO contents increase from the core to the rim (Table 1 and Figs. 3 and 4). Mg# in transitional zone, i.e. between the core and the rim, overlaps with the olivines from the pyroxenite xenoliths entrained in Fangcheng basalts. The rims have large compositional variations (Mg#=76~83), in which some olivines have very low Mg#, close to Mg# of olivine phenocrysts of the host rocks. One important feature is that the larger grains (600~900 μm) generally have high and relatively constant Mg# (88–92) in the core and the rim is very thin (about 100 μm), where the Mg# decreases rapidly (Fig. 3). In contrast, the smaller grains (200~500 μm) generally have low and variable Mg# (83~87) in the narrow core and the Mg# decreases gradually from the core to the rim. Olivine phenocrysts are low in Mg#, all <80.5 (75~80) and high in MnO contents (0.23~0.47 wt.%) (Fig. 5), and do not show clearly compositional zonation. Their Mg# variations are less than 2%

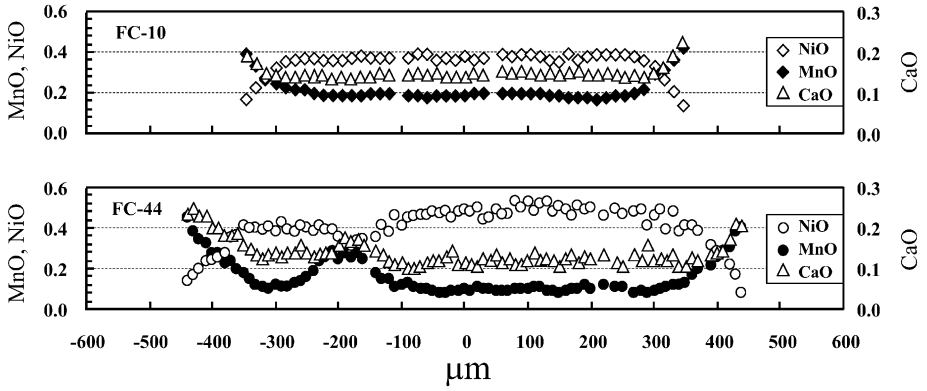

Fig. 4. Compositional traverses for two representatives of zoned olivines (FC-10, FC-44). Oxide expresses as wt.%.

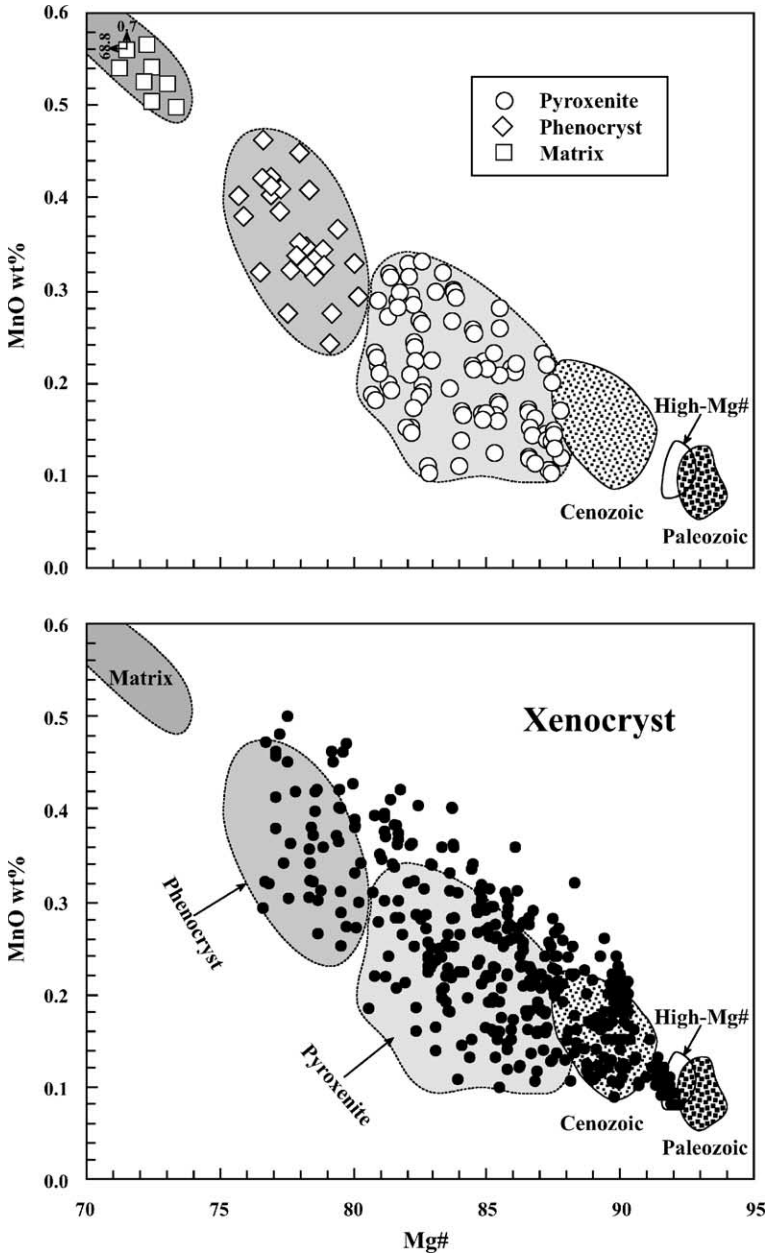

Fig. 5. Mg# versus MnO wt.% in olivines. Paleozoic and Cenozoic represents olivines from xenocrysts entrained in Paleozoic Mengyin kimberlites and from peridotitic xenoliths entrained in Cenozoic basalts on the Sino-Korean craton (Qixia, Shanwang, Penglai, and Hebi), respectively [16,19]. High-Mg# represents olivines from high-Mg peridotites entrained in Cenozoic Hebi basalts, Henan Province [19]. Pyroxenite represents olivines from olivine clinopyroxenite xenoliths from Fangcheng basalts.

from the core to the rim. Olivines in matrix have extremely low Mg# (mainly in the range of 71~74 and can be as low as 68.8) and posses very high MnO contents (0.49–0.70). Olivines in the pyroxenite xenoliths are relatively high in Mg# (80.5~88) and MnO content (0.1~0.34 wt.%) (Fig. 5).

7. Discussion

7.1. Are zoned olivines xenocrysts?

Larger grains of zoned olivines have the Mg# in their cores similar to the Mg# of olivines from peridotitic xenoliths from Cenozoic basalts of the Sino-Korean craton, such as those from high-Mg# peridotitic xenoliths from Cenozoic Hebi basalts, Henan province (Fig. 5). The Mg# in rims are close to the Mg# of generally non-zoned olivine phenocrysts of the host basalts. These features, together with the crystal shapes, strongly suggest that these apparently zoned and rounded olivines are xenocrysts, rather than early-crystallized phenocrysts. The fact that the cores of olivine xenocrysts have much higher Mg# and larger grain sizes than olivines from olivine pyroxenite xenoliths entrained in the same basalts (Fig. 5) manifests that these olivine xenocrysts were not disaggregated from mantle pyroxenites, but should be disaggregated from mantle peridotites.

7.2. Formation and preservation

Olivine with such zoned texture is believed to be formed by the olivine-melt reaction [3–7]. When high-temperature (≥ 1200 °C) basaltic magma trapped olivine crystal, compositional disequilibria between olivine and melt may cause erosion and reaction between the olivine and the host magma. As a result, the rims of olivine approach equilibrium with the composition of host magma. This olivine-melt reaction could happen in ion diffusion, i.e. in the form of Mg–Fe exchange.

$$(Mg, Fe)_2SiO_4\ (\text{forsterite}) + \text{Melt}\ (\text{primary}) = (Mg, Fe)_2SiO_4\ (\text{chrysolite}) + \text{melt}\ (\text{derivative}).$$

When melt temperature decreased to a certain degree after eruption, the reaction or diffusion was terminated, and thus disequilibrated texture was preserved. The reaction may be terminated before matrix olivines crystallized, as manifested by the fact that the rims of olivine xenocrysts do not show the similar compositions to those matrix olivines. Since Mg and Fe diffusion in olivine is very fast (Mg diffusion coefficient in olivine at 12 kb and 1350 °C $\approx 1.4 \times 10^{-8}$ cm^2/s) [6,32–34], the occurrence of such an excellent olivine zonation demonstrates that the reaction happened at very short time period, probably in a few weeks to months according to the Mg–Fe interdiffusion model [35]. This provides further evidence for rapid eruption of the basalts in the region, consistent with the results obtained from the geochemical studies on basalts themselves [20]. Preservation of zoned texture of olivines requires the rapid ascending of the magma. This explains why zoned olivine xenocrysts are widespread in global kimberlites and few basalts, but not in mafic intrusion.

7.3. Peridotite-melt reaction

Peridotite-melt/magma reaction is common in ophoilites [36–38], orogenic massifs [39], ultramafic intrusive complexes [40–42], and mantle peridotitic xenoliths [42,43]. The reaction has been demonstrated in a number of experimental studies [44–46]. In ophiolites and orogenic massifs, the reaction is characterized by dissolution of orthopyroxene and precipitation of olivine, sometimes in accompany with the generation of clinopyroxenite veins. This peridotite-melt reaction model well accounts for the formation of dunites in some ophiolites [36–38] and orogenic massifs [39] and podiform chromitites in ophiolites [36–38]. The reaction can be described as: (I), Orthopyroxene + Melt 1 = Olivine + SiO_2 (Melt 2) (+ clinopyroxene). In contrast, another type of peridotite-melt reaction: (II), Olivine + SiO_2 (Melt 1) (+clinopyroxene)= Orthopyroxene (+Melt 2), dominantly occurs in ultramafic intrusive complexes [40–42] and mantle peridotite xenoliths [42,43]. This reaction is typified by the dissolution of olivine (and clinopyroxene) and precipitation of orthopyroxene and is used to interpret the formation of some harzburgites in mantle peridotitic xenoliths and ultramafic intrusive complexes. The latter reaction model could be widespread in old lithospheric mantle [42,43,47,48]. Based on detailed mineralogical and petrological studies on mantle peridotite xenoliths worldwide, Kelemen et al. [42] found many mantle peridotites are too high in orthopyroxenes (SiO_2-rich) and LREE/HREE ratios, which are inconsistent with the residuum left by extraction of basaltic magma from the primitive mantle. Thus they proposed that these harzburgites were considerably affected by mantle metasomatism. Based on the

studies on the concentric ultramafic intrusive complex (dunite, harzburgite, lherzolite, plagioclase lherzolite) from the northern California, these authors [40–42] argued that this complex provides the first geological evidence for the existence of metasomatic harzburgite. Zhang et al. [43,48] on the basis of the studies on the polymict peridotitic xenoliths from South Africa identified the orthopyroxene of metasomatic origin, thus they provided the first petrological evidence for the existence of metasomatic harzburgites in the lithospheric mantle. More importantly, there are large compositional differences between the metasomatic orthopyroxene and the primary or non-metasomatic orthopyroxene [43]. Interestingly, the above two types of reaction (reaction I: clinopyroxene replaced orthopyroxene and precipitation of olivine and reaction II: orthopyroxene replaced clinopyroxene and dissolution of olivine) occur in one polymict peridotitic xenoliths [48]. Both temperature-pressure calculation of mineral phases [43] and mineral volume changes involving olivine during the reaction [47] demonstrate that reaction I tends to happen at shallower level and reaction II at deeper depth. This is consistent with the fact that the reactant dunites mainly occur in ophiolites [36–38] and orogenic massifs [39] whereas metasomatic harzburgites in ultramafic intrusive complexes and mantle peridotitic xenoliths [42,43]. Based on the positive co-relation between Ni content in olivine and orthopyroxene mode of peridotites, olivine volume changes during the reaction and porous flow features, Kelemen et al. [47] further suggested that reaction I is unlikely widespread in the lithospheric mantle, but reaction II is most likely ubiquitous in old lithospheric mantle, namely the major type of peridotite-melt reaction in the lithospheric mantle.

Another important fact is that no matter what type of reaction happened, the peridotite-melt reaction led not only to changes in modal contents of different mineral phases of peridotites (olivine, orthopyroxene, clinopyroxene, spinel/garnet), but also inevitably to compositional changes within mineral phases. The latter has not been paid enough attention. As stated earlier, orthopyroxene prior to and after the reaction has a large compositional variation [43]. However, how does the composition change of the most important mineral phase in peridotite, i.e. olivine during the reaction? Large compositional variations exist in olivines of South African polymict peridotitic xenoliths (Mg# in large porphyroclastic crystal=92–95 and in small crystal=87–91). Since the polymict peridotites are hybrid, with minerals and rocks of different origins brought together by mantle shear [43,48] and they do not show compositional zonation, we believed that olivine porphyroclasts were refractory residuum and small olivines with low Mg# were crystallized from melts. Presence of clearly zoned olivine xenocrysts in Fangcheng basalts provides us natural samples to investigate the olivine compositional changes during the peridotite-melt reaction. It is obvious that the result of the reaction depends on the percolative melt composition. In general, melt is rich in Si, Ca, Fe, Mn and poor in Mg and Ni, relative to lithospheric mantle peridotites. Reaction most likely results in the evolution of peridotites towards Fe, Mn enrichment and Mg, Ni depletion, i.e. to the formation of low-Mg olivines. Because larger compositional difference between mantle minerals and the melt will enhance the reactions, infiltration of more silicic crustal melt into the lithospheric mantle rather than basaltic melt could led to more severe peridotite-melt reaction, which forms more fertile lithospheric mantle.

7.4. Implication for lithosphere evolution

On the Sino-Korean craton, olivine xenocrysts in Paleozoic kimberlites have very high Mg# (92~95, Fig. 5), which is consistent with the value of olivines from kimberlite-borne peridotitic xenoliths from the same localities [17,19]. This demonstrates that highly refractory lithospheric mantle indeed existed beneath the Archaean Sino-Korean craton, comparable with the old lithospheric mantle underneath the Archaean cratons worldwide (such as Kaapvaal and Siberia) [49–51]. This highly refractory lithospheric mantle beneath the region was preserved at least till the late Paleozoic. Although the occurrence of high Mg# peridotitic xenoliths from the Cenozoic basalts from Hebi, Henan Province [19] manifests that this highly refractory lithospheric mantle remained beneath certain areas of the craton till the Cenozoic time, the majority of this highly refractory mantle peridotite disappeared in late Cretaceous [21,52]. This is shown by the compositions of olivines from the mantle peridotites entrained in the late Cretaceous basalts: they all have Mg# less than 92, predominantly falling in the range of

88–91. Now the question is how the highly refractory lithospheric mantle peridotites disappeared?

Process for zoned olivine formation can provide some important implications for the above question. As mentioned above, the zoned olivine xenocrysts are minerals disaggregated from lithospheric mantle peridotites. Thus, the core composition in larger grains can record the composition (Mg# = 88–92) of olivines of the lithospheric mantle peridotites. This manifests that the lithospheric mantle at 125 Ma was significantly different from the old highly refractory lithospheric mantle, but had some similarities to the mantle peridotitic xenoliths entrained in younger basalts [21,52]. Preservation of the zoned olivine may suggest that mineral-melt reactions could have been widespread in lithospheric mantle. The reactions led not only to the increase of orthopyroxene contents of the peridotite, but also to the transformation of the high Mg# peridotites to the low Mg# peridotites. The clinopyroxenite veins in the peridotites represent residual melt trapped in the lithospheric mantle, which is relatively rich in Ca and Al [20]. Because the mineral-melt reaction is easy to reach chemical equilibrium under lithospheric mantle conditions, zoned olivines are generally not preserved. Finding of such clearly zoned olivine xenocrysts may indicate that the reaction between mantle peridotite and the melt is an important mechanism for the lithospheric mantle replacement, which led to the transformation of the nature of the lithospheric mantle beneath the Sino-Korean craton from a highly refractory one in the Paleozoic to a fertile one (peridotites + pyroxenites) in the late Cretaceous. The trace element and isotopic compositions of the transformed lithospheric mantle depend on the melt composition involved in the reaction [20,21]. Finally, it must be mentioned that the melt responsible to the transformation from the high Mg# peridotitic mantle to low Mg# peridotites was not related to the melt that crystallized the host Fangcheng basalts.

8. Conclusion

Preservation of zoned olivine xenocrysts from Mesozoic Fangcheng tholeiites provides evidence for the existence of olivine-melt reaction in the lithospheric mantle underneath the southeastern Sino-Korean craton. Comparison with olivines from Paleozoic kimberlite and Cenozoic basalt borne peridotites and/or xenocrysts inferred that this reaction was widespread in the lithospheric mantle beneath the southeastern portion of the Sino-Korean craton, which led to transformation of the old refractory lithospheric mantle to the young fertile one. We conclude that this peridotite-melt reaction was the major mechanism of the lithospheric replacement in the Mesozoic time.

Acknowledgements

This research was financially supported by the Natural Science Foundation of China (40225009) and Chinese Academy of Sciences (KZCX3-SW-135). N. T. Kita and Y. Morishita are thanked for providing the EPMA facility and their assistances in the EPMA analyses at the Geological Survey of Japan, National Institute of Advanced Industrial Science and Technology.

References

[1] P.C. Burnley, H.W. Green, Stress dependence of the mechanism of the olivine-spinel transformation, Nature 338 (1989) 753–756.
[2] C.R. Bina, Olivine emerges from isolation, Nature 392 (1998) 650–653.
[3] S. Maaløe, B. Hansen, Olivine phenocrysts of Hawaiian olivine Tholeiite and Oceanite, Contrib. Mineral. Petrol. 81 (1982) 203–211.
[4] D.A. Clague, W.S. Weber, J.E. Dixon, Picritic glasses from Hawaii, Nature 353 (1991) 553–556.
[5] A.V. Sobolev, N. Shimizu, Ultra-depleted primary melt included in an olivine from the Mid-Atlantic Ridge, Nature 363 (1993) 151–154.
[6] N. Nakamura, Residence time and crystallization history of nickeliferous olivine phenocrysts from the northern Yatsugatake volcanoes, Central Japan: application of a growth and diffusion model in the system Mg-Fe-Ni, J. Volcanol. Geotherm. Res. 66 (1995) 81–100.
[7] A. Klügel, Prolonged reactions between harzburgite xenoliths and silica-undersaturated melt: implications for dissolution and Fe–Mg interdiffusion rates of orthopyroxene, Contrib. Mineral. Petrol. 141 (2001) 1–14.
[8] T. Lidaka, D. Suetsugu, Seismological evidence for metastable olivine inside a subducting slab, Nature 256 (1992) 593–595.
[9] T. Mizukami, S.R. Wallis, J. Tamamoto, Natural examples of olivine lattice preferred orientation patterns with a flow-normal a-axis maximum, Nature 427 (2004) 432–436.

[10] J. Ando, Y. Shibata, Y. Okajima, K. Kanagawa, M. Furusho, N. Tomioka, Striped iron zoning of olivine induced by dislocation creep in deformed peridotites, Nature 414 (2001) 893–895.
[11] S. Lebedev, S. Chevrot, R.D. van der Hilst, Seismic evidence for olivine phase changes at the 410- and 660-kilometer discontinuities, Science 296 (2002) 1300–1302.
[12] W.L. Griffin, S.Y. O'Reilly, C.G. Ryan, Composition and thermal structure of the lithosphere beneath south Africa, Siberia and China: proton microprobe studies, International Symposium on Cenozoic Volcanic Rocks and Deep-Seated Xenoliths of China and its Environs, Beijing, 1992, pp. 65–66.
[13] W.L. Griffin, A.D. Zhang, S.Y. O'Reilly, C.G. Ryan, Phanerozoic evolution of the lithosphere beneath the Sino-Korean Craton, in: M.F.J. Flower, S.L. Chung, C.H. Lo, T.Y. Lee (Eds.), Mantle dynamics and plate interactions in East Asia, Geodynamics Series, vol. 27, American Geophysical Union, 1998, pp. 107–126.
[14] M.A. Menzies, W.M. Fan, M. Zhang, Palaeozoic and Cenozoic lithoprobes and the loss of >120 km of Archaean lithosphere, Sino-Korean craton, China, in: H.M. Prichard, T. Alabaster, N.B.W. Harris, C.R. Neary (Eds.), Magmatic processes and plate tectonics, Geol. Soc. Spel. Pub., vol. 76, 1993, pp. 71–78.
[15] M.A. Menzies, Y.G. Xu, Geodynamics of the North China Craton, in: M.F.J. Flower, S.L. Chung, C.H. Lo, T.Y. Lee (Eds.), Mantle Dynamics and Plate Interactions in East Asia, Geodynamics Series, vol. 27, American Geophysical Union, 1998, pp. 155–165.
[16] W.M. Fan, H.F. Zhang, J. Baker, K.E. Jarvis, P.R.D. Mason, M.A. Menzies, On and off the North China Craton: where is the Archaean keel? J. Petrol. 41 (2000) 933–950.
[17] Y.G. Xu, Thermo-tectonic destruction of the Archean lithospheric keel beneath the Sino-Korean Craton in China: evidence, timing and mechanism, Phys. Chem. Earth (A) 26 (2001) 747–757.
[18] S.Y. O'Reilly, W.L. Griffin, Y.H. Poudjom Djomani, P. Morgan, Are lithospheres forever? Tracking changes in sub-continental lithospheric mantle through time, GSA Today 11 (4) (2001) 4–10.
[19] J.P. Zheng, S.Y. O'Reilly, W.L. Griffin, F.X. Lu, M. Zhang, N.J. Pearson, Relict refractory mantle beneath the eastern North China block: significance for lithosphere evolution, Lithos 57 (2001) 43–66.
[20] H.F. Zhang, M. Sun, X.H. Zhou, W.M. Fan, M.G. Zhai, J.F. Yin, Mesozoic lithosphere destruction beneath the North China Craton: evidence from major, trace element, and Sr-Nd-Pb isotope studies of Fangcheng basalts, Contrib. Mineral. Petrol. 144 (2002) 241–253.
[21] H.F. Zhang, M. Sun, X.H. Zhou, M.F. Zhou, W.M. Fan, J.P. Zheng, Secular evolution of the lithosphere beneath the eastern North China Craton: evidence from Mesozoic basalts and high-Mg andesites, Geochim. Cosmochim. Acta 67 (2003) 4373–4387.
[22] H.F. Zhang, M. Sun, M.F. Zhou, W.M Fan, X.H. Zhou, M.G. Zhai, Highly heterogeneous Late Mesozoic lithospheric mantle beneath the North China Craton: evidence from Sr-Nd-Pb isotopic systematics of mafic igneous rocks, Geol. Mag. 141 (2004) 55–62.
[23] W.M. Fan, F. Guo, Y.J. Wang, M. Zhang, Late Mesozoic volcanism in the northern Huaiyang tectono-magmatic belt, central China: partial melts from a lithospheric mantle with subducted continental crust relicts beneath the Dabie orogen, Chem. Geol. 209 (2004) 27–48.
[24] G.C. Zhao, S.A. Wilde, P.A. Cawood, M. Sun, Archean blocks and their boundaries in the North China Craton: lithological, geochemical, structural and P-T path constraints and tectonic evolution, Precambrian Res. 107 (2001) 45–73.
[25] S.G. Li, Y.L. Xiao, D.L. Liou, Y.Z. Chen, N.J. Ge, Z.Q. Zhang, S.S. Sun, B.L. Cong, R.Y. Zhang, S.R. Hart, S.S. Wang, Collision of the North China and Yangtze Blocks and formation of coesite-bearing eclogites — timing and processes, Chem. Geol. 109 (1993) 89–111.
[26] Q.R. Meng, G.W. Zhang, Geologic framework and tectonic evolution of the qinling orogen, central China, Tectonophysics 323 (2000) 183–196.
[27] A.M.C. Şengör, B.A. Natal'in, V.S. Burtman, Evolution of the altaid tectonic collage and Palaeozoic crustal growth in Eurasia, Nature 364 (1999) 299–307.
[28] S.T. Xu, A.J. Okay, S. Ji, A.M.C. Sengör, W. Su, Y. Liu, L. Jiang, Diamond from Dabie Shan metamorphic rocks and its implication for tectonic setting, Science 256 (1992) 80–82.
[29] J.B. Liu, K. Ye, S. Maruyama, B.L. Cong, H.R. Fan, Mineral inclusions in zircon from gneisses in the ultrahigh-pressure zone of the Dabie Mountains, China. J. Geol. 109 (2001) 523–535.
[30] K. Ye, B.L. Cong, D.N. Ye, The possible subduction of continental material to depths greater than 200 km, Nature 407 (2000) 734–736.
[31] J.W. Xu, The Tancheng-Lujiang Wrench fault system, John Wiley and Sons Ltd, Chichester, England, 1993, 279 pp.
[32] M. Brearley, C.M. Scarfe, Dissolution rates of upper mantle minerals in an alkali basalt melt at high pressure: an experimental study and implications for ultramafic xenolith survival, J. Petrol. 27 (1986) 1157–1182.
[33] S. Chakraborty, Rates and mechanisms of Fe–Mg interdiffusion in olivine at 980°–1300 °C, J. Geophy. Res. 102 (1997) 12317–12331.
[34] S.A.T. Redfern, C.M.B. Henderson, B.J. Wood, R.J. Harrison, K.S. Knight, Determination of olivine cooling rates from metal-cation ordering, Nature 381 (2002) 407–409.
[35] A. Klügel, K.A. Hoernle, H.U. Schmincke, J.D.L. White, The chemically zoned 1949 eruption on La Palma (Canary Islands): petrologic evolution and magma supply dynamics of a rift zone eruption, J. Volcanol. Geotherm. Res. 105 (2000) 5997–6016.
[36] M.F. Zhou, P.T. Robinson, J. Malpas, Z.J. Li, Podiform chromitites in Luobusa ophiolite (Southern Tibet): implications for melt-rock interaction and chromite segregation in the upper mantle, J. Petrol. 37 (1996) 3–21.
[37] M.F. Zhou, P.T. Robinson, J. Malpas, J. Aitchison, M. Sun, W.J. Bai, X.F. Hu, J.S. Yang, Melt/rock interaction and melt evolution in the Sartohay high-Al chromite deposits of the

Dalabute ophiolite (NW China), J. Asian Earth Sci. 19 (2001) 517–534.
[38] P.B. Kelemen, Reaction between ultramafic rock and fractionating basaltic magma I. Phase relations, the origin of calc-alkaline magma series, and the formation of discordant dunite, J. Petrol. 31 (1990) 51–98.
[39] J.L. Bodinier, G. Vasseur, J. Vernieres, J. Dupuy, J. Fabries, Mechanisms of mantle metasomatism: geochemical evidence from the Lherz orogenic peridotite, J. Petrol. 31 (1990) 597–628.
[40] J.E. Quick, The origin and significance of large, tabular dunite bodies in the Trinity peridotite, Northern California, Contrib. Mineral. Petrol. 78 (1981) 413–422.
[41] P.B. Kelemen, M.S. Ghiorse, Assimilation of peridotite in zoned calc-alkaline plutonic complexes: evidence from the Big Jim Complex, Washington Cascades, Contrib. Mineral. Petrol. 94 (1986) 12–28.
[42] P.B. Kelemen, J.B. Dick, J.E. Quick, Formation of harzburgite by pervasive melt/rock reaction in the upper mantle, Nature 358 (1992) 635–640.
[43] H.F. Zhang, M.A. Menzies, J. Gurney, X.H. Zhou, Cratonic peridotites and silica-rich melts: diopside-enstatite relationships in polymict xenoliths, Kaapvaal, South Africa, Geochim. Cosmochim. Acta 65 (2001) 3365–3377.
[44] M.R. Fisk, Basalt-magma interactions with harzburgite and the formation of high magnesium andesites, Geophys. Res. Lett. 13 (1986) 467–470.
[45] M.J. Daines, D.L. Kohlstedt, The transition from porous to channelized flow due to melt/rock reaction during melt migration, Geophys. Res. Lett. 21 (1994) 145–148.
[46] P.B. Kelemen, D.M. Joyce, J.D. Webster, J.R. Holloway, Reaction between ultramafic rock and fractionating basaltic magma II. Experimental investigation of reaction between olivine tholeiites and harzburgite at 1150–1050 °C and 5 kar, J. Petrol. 31 (1990) 99–134.
[47] P.B. Kelemen, S.R. Hart, Bernstein, Silica enrichment in the continental upper mantle via melt/rock reaction, Earth Planet. Sci. Lett. 164 (1998) 387–406.
[48] H.F. Zhang, M.A. Menzies, D. Mattey, Mixed mantle provenance: diverse garnet compositions in polymict peridotites, Kaapvaal craton, South Africa, Earth Planet. Sci. Lett. 216 (2003) 329–346.
[49] F.R. Boyd, Compositional distinction between oceanic and cratonic lithosphere, Earth Planet. Sci. Lett. 96 (1989) 15–26.
[50] F.R. Boyd, N.P. Pokhilenko, D.G. Pearson, S.A. Mertzman, N.V. Sobolev, L.W. Finger, Composition of the Siberian cratonic mantle: evidence from Udachnaya peridotite xenoliths, Contrib. Mineral. Petrol. 128 (1997) 228–246.
[51] O.F. Gaul, W.L. Griffin, S.Y. O'Reilly, N.J. Pearson, Mapping olivine composition in the lithospheric mantle, Earth Planet. Sci. Lett. 182 (2000) 223–235.
[52] J. Yan, J.F. Chen, Z. Xie, T.X. Zhou, Mantle xenoliths from Late Cretaceous basalt in eastern Shandong Province: new constraint on the timing of lithospheric thinning in eastern China, Chin. Sci. Bulletin 48 (19) (2003) 2139–2144.